Proceedings of the 2022 Winter Simulation Conference
B. Feng, G. Pedrielli, Y. Peng, S. Shashaani, E. Song, C.G. Corlu, L.H. Lee, E.P. Chew, T. Roeder, and P. Lendermann, eds.

URBAN SUBSURFACE MAPPING VIA DEEP LEARNING BASED GPR DATA INVERSION

Mengjun Wang
Da Hu
Shuai Li

Department of Civil and Environmental Engineering
The University of Tennessee
851 Neyland Drive
Knoxville, TN 37996, USA

Jiannan Cai

School of Civil & Environmental Engineering and Construction Management
The University of Texas at San Antonio
501 W César E Chávez Blvd
San Antonio, TX 78207, USA

ABSTRACT

Accurate mapping of urban subsurface is essential for managing urban underground infrastructure and preventing excavation accidents. Ground-penetrating radar (GPR) is a non-destructive test method that has been used extensively to locate underground utilities. However, existing approaches are not able to retrieve detailed underground utility information (e.g., material and dimensions) from GPR scans. This research aims to automatically detect and characterize buried utilities with location, dimension, and material by processing GPR scans. To achieve this aim, a method for inverting GPR data based on deep learning has been developed to directly reconstruct the permittivity maps of cross-sectional profiles of subsurface structure from the corresponding GPR scans. A large number of synthetic GPR scans with ground-truth permittivity labels were generated to train the inversion network. The experiment results indicated that the proposed method achieved a Mean Absolute Error of 0.53, a Structural Similarity Index Measure of 0.91, and an R^2 of 0.96.

1 INTRODUCTION

The National Academy of Engineering (NAE) has identified "restore and improve urban infrastructure" as a grand engineering challenge and acknowledged that "mapping and labeling buried infrastructure" is a prerequisite for improving it and helping avoid damaging it (NAE 2019). A vast network of pipes, cables and conduits are buried in urban subsurface with unknown locations (Talmaki and Kamat 2014). The records of the buried infrastructure are often unavailable, incomplete, and inaccurate (Thomas et al. 2009), causing an endless litany of incidents. The 12794 significant pipeline incidents that occurred in the United States from 2002 to 2021 resulted in 276 fatalities, 1147 injuries, and over 10 billion in property damage (PHMSA 2021). About 40% of the incidents were related to poor locating practices (Metje et al. 2015). Therefore, there is a critical need to map and label the underground utility features.

Traditionally, the utility owners marked the utility location with spray paint or flags to avoid pipeline accidents (Su et al. 2013). However, this method always cannot accurately point out the precise utility position but only an approximate range, and the mark could be damaged along time. To address this issue, Ground-penetrating radar (GPR) has been used in underground utility detection and characterization (Li et al. 2016). GPR is a non-destructive testing method that utilizes the different electromagnetic properties of underground materials to detect object regions by emitting high-frequency electromagnetic waves (Sterling et al. 2009). Cylindrical underground utilities are typically recognized as hyperbolas in GPR scans. In recent years, there has been an increasing interest in developing hyperbola detection methods from GPR scans to

position the underground utility (Li et al. 2015). The GPR scan has also been used to measure quantitative information about buried utilities such as shape and size (Pasolli et al. 2009; Singh and Nene 2013).

Despite the great potential of GPR for underground utility detection, existing hyperbolic approaches are difficult to recognize the size and material of a buried utility. Size and material information can be used to infer the types of buried underground utilities. The lack of such information could give rise to greater concerns in urban excavation projects. The deep neural network has been widely used in many areas of research and achieve promising results. To address this limitation, this paper proposed a novel approach to urban underground mapping through deep learning based on the inversion of GPR data. The proposed method can detect the position of a buried utility and get detailed information about its material and size. The following section provides an overview of existing GPR data processing approaches.

2 LITERATURE REVIEW

Urban underground utility mapping is an essential but challenging task, with an increasing number of underground infrastructures. Traditionally, metal detectors are frequently used to locate pipelines buried in construction sites with high accuracy (Bruschini 2000; Das 2006). However, the detection and clearance of metal detectors depend heavily on the use of manual methods which is labor and time-consuming. On the other hand, the use of PVC pipes has grown considerably in recent years (Folkman 2014), so the conventional detection method becomes unsuited. Researchers have proposed many trenchless technologies to precisely locate underground infrastructure and find out their size and location. Ground-penetrating radar (GPR) has played an important role in underground utility detection as it can be used to detect metallic and non-metallic objects (Liu et al. 2021). For example, GPR has been used to detect and reconstruct survivable void space in disaster rubbles (Hu et al. 2019; Hu et al. 2022). Some researchers used the relationship between GPR hyperbole parameters in radargram and geometrical characteristics of cylindrical objects (horizontal and perpendicular position, radius) to locate the underground utilities (Ahmadi and Fathianpour 2017; Rajiv et al. 2017).

Yang et al. (2014) proposed a method that extracts the hyperbola from the image to compute the position and diameter of the pipeline using a hyperbolic asymptote. It is suitable for processing GPR data in real-time. Sagnard and Tarel (2016) proposed a matching model based on a semi-automatic hyperbola detection algorithm with no preliminary training period to reconstruct the parameters of underground targets, thus mitigating the tedious training process. Rohman and Nishimoto (2021) applied pattern matching techniques in three shapes of infrastructures: circle, square, and triangle, extending the available environments. Although the above algorithms could detect thin pipes or strips in the soil, they still need the user's help due to the diversity of hyperbola signatures as GPR images contain lots of noises. Furthermore, users need to define various threshold values for the matched template to suit different target detection areas. There is still enormous room for improvement in positioning precision for these hyperbola-based template matching methods for these reasons.

With the advancement of computer vision, convolutional neural network (CNN) has become dominant in various computer vision tasks, such as material classification (Hu and Li 2022), affordance segmentation (Hu et al. 2020), and object detection and segmentation (Westwańska and Respondek 2019, 2020). Moreover, many researchers have developed deep learning based methods for detecting and characterizing underground infrastructure. Feng et al. (2020) proposed DepthNet extracts and denoises the hyperbola features in B-scan data to predict the dielectric to determine the depth of targets. Hou et al. (2021) developed the Mask Scoring R-CNN (MS R-CNN) to segment and analyze hyperbolic signatures of subsurface targets in GPR scans. Yamaguchi et al. (2021) combined a 3-D convolutional neural network and Kirchhoff migration searched for the box-by-box radar image and extracted the peaks of the hyperbola. Thus, they claim that their algorithm could provide a clear 3-D pipe map in a reasonable calculation time. All of the above research focused on determining the size and position of subsurface utilities, but little attention was paid to the material of the pipeline. The material of underground utilities has a great impact on the excavation work, as engineers could make a specific plan according to different pipelines under the target

area to perform safe and efficient excavation work. However, this point has been overlooked by most existing studies of subsurface mapping.

Some researchers noticed the importance of underground infrastructure materials these days. Permittivity reconstruction is useful for this process. Qin et al. (2021) presented a probabilistic inversion method using a sliding window and Markov chain Monte Carlo simulation with Bayesian inference based on the relative permittivity and electric conductivity values from GPR waveform data. Liu et al. (2021) proposed a DNN architecture that uses the fuse characteristics of several aligned traces on B-Scan data to reconstruct the permittivity map of tunnel linings. Ji et al. (2021) utilized a temporal compression operation and a global feature encoder to reconstruct permittivity images from GPR data at different central frequencies. The main drawback of the above research is the ignorance of the dielectric parameters in different underground layers. Specifically, the time-domain radargram was directly aligned with the spatial-domain subsurface permittivity map, which could cause a depth gap between prediction and ground truth. Moreover, it was assumed that the environmental context was relatively homogenous in these studies, compromising its applicability in the real world. To address these limitations, Hu et al.(2022) applied a neural network with an encoder-decoder structure to directly reconstruct the permittivity maps of collapsed structures in the aftermath of disasters. However, the generalizability of this method in referring subsurface pipes remains unexplored. Our study aims to address these knowledge gaps.

3 METHODOLOGY

Figure 1 presents the architecture of the proposed network. The proposed deep learning network is adapted from the DeepLabv3+ architecture (Chen et al. 2018). The encoder-decoder structure is integrated with Atrous Spatial Pyramid Pooling (ASPP) module to encode multi-scale contextual information.

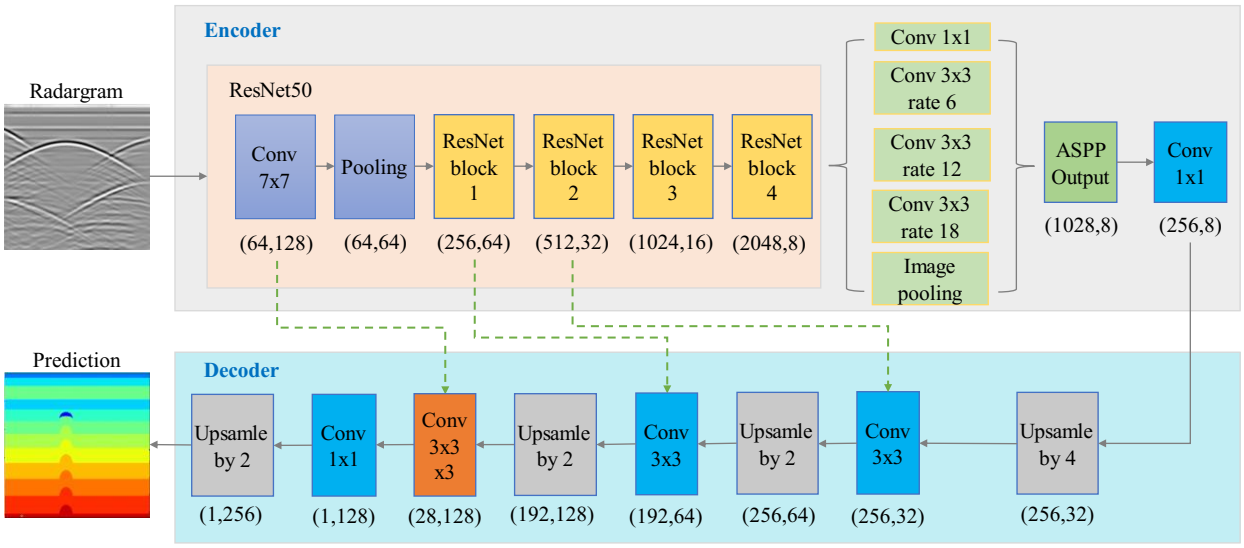

Figure 1: Overview of the methodology.

The backbone encoder is built based on the ResNet50 network. The obtained feature maps are fed into the ASPP module to extract multi-scale features using multiple parallel filters with different dilated rates. This process can improve inversion accuracy with the ability to account for different object scales. The ASPP module contains a 1×1 convolution layer, three 3×3 convolution layers, and global average pooling. The sampling rate of the four convolution layers is 1, 6, 12, and 18, respectively. The batch normalization and ReLU activation layer are added followed by each convolution layer and pooling layer. The output of a single layer from the ASPP module is 256 channels. The five layers are concatenated together with 1280

channels. Subsequently, a 1×1 convolution with 256 output channels is applied to the concatenated layer to obtain a high-level feature map. At the decoder, upsampling and convolutions are performed to enlarge the feature map and obtain the final prediction. Each of the low-level features extracted from Resnet blocks would be passed to one 1×1 convolutional layer followed by batch normalization layer, ReLU activation layer, and dropout. Then these processed features are integrated into the corresponding high-level features in the decoder. The designs of the Resnet50 backbone and decoder are elaborated below.

Encoder: The ResNet50 backbone contains 5 stages (He et al. 2016) The first stage consists of one convolution layer with kernel size 7×7, one batch normalization layer, one ReLU activation layer, and one max-pooling layer. This stage is mainly used to process the input data. The spatial dimension of the output from stage 1 is 64 with a channel number of 64. The following four stages are ResNet residual blocks with a block number of 3, 4, 6, and 3, respectively. Each block contains three convolutional layers, one batch normalization, and one ReLU activation layer. In each stage, the output channel would double and the size of the feature map reduced to half from stage 2 to stage 5.

Decoder: The low-level features obtained from the ResNet block 2 of the backbone module is passed into one 1×1 convolutional layer followed by one batch normalization layer and one Relu activation layer. At the same time, the high-level features obtained from the 1×1 convolution with 256 output channels in the encoder are up-sampled through bilinear interpolation whose scale factor is 4. The two feature maps are concatenated together to utilize low-level features. The concatenated feature map is fed into one 3 × 3 convolutional layer followed by one batch normalization layer and one Relu activation layer. Sequentially, the output is applied in the bilinear interpolation up-sample layer followed by one 3×3 convolutional layer and another up-sample layer. The intermediary feature map would be further passed into three 3×3 convolutional layer blocks and one 1×1 convolutional layer block. Finally, the predicted permittivity map is generated with the same size as the original radargram after up-sampling by 2.

4 DATA PREPARATION

4.1 Simulation Parameters

In this study, numerical simulation is used to generate synthetic GPR scans as it is nearly impossible to get a ground-truth permittivity map for real GPR data. Collecting an abundance of real GPR data is very time-consuming and requires a great deal of work. And also the material of the natural subgrade is always heterogeneous and unpredictable. In addition, the dielectric properties of these materials would vary with temperature and humidity. Building permittivity maps based on real scenes would be very difficult. Furthermore, the simulation can generate a large number of synthetic GPR scans along with ground-truth permittivity labels generated to train the deep learning network. The gprMax (Warren et al. 2016) simulator is adopted to generate synthetic GPR scans, which is a well-accepted GPR simulator.

To reflect a realistic underground pipe system, the simulated subsurface scenarios refer to the design standard of urban roads and underground utilities. The typical flexible pavement in urban areas is used as the subsurface background, which consists of surface, base course, subbase course, and subgrade layer. Table 1 shows the thickness range of each layer.

Table 1: Depth parameters of the background (TDOT 2021).

Road layer	Thickness (cm)
Surface	10-18
Base course	13-30
Subbase course	13-30
Subgrade layer	The rest

The five most common buried utilities under urban sidewalks are selected that are gas pipe, sewer pipe, water pipe, electrical wire, and optical cable. The material of these buried utilizes could be PVC, concrete,

or iron. In addition, the size, depth, and installation requirements are also different. Table 2 shows the radius and depth range of the five types of buried utilities. Moreover, there are clearance requirements for these pipes according to their functionalities.

Table 2: Underground pipelines spatial setting (ASME 2016).

Utility lines	**Inside radius (cm)**	**Outside radius (cm)**	**Depth (cm)**	**Remark**
Gas lines	(1,14)	(1,15)	61 below	The 30.5 cm vertical clearance from water and sewer pipelines
Electrical wire	N/A	(2,5)	61 below	The 30.5 cm vertical clearance from water and sewer pipelines
Water lines	(1,28)	(3,30)	91.4 below	The 45.7 cm vertical clearance from sewage lines
Sewage lines	(3,19)	(5,20)	61-91.4 below	The 45.7 cm vertical clearance from water lines
Optical cable	N/A	(1,2)	30.5 below	The 30.5 cm vertical clearance from water and sewer pipelines

Table 3 shows the relative permittivity ranges of different objects that are used to generate underground pipelines and road structures. The relative permittivity values are uniformly randomized given the range for each object.

Table 3: Permittivity values of different materials.

Object	**Permittivity**
PVC	3-5 (Hilario et al. 2019)
Concrete	5-10
Clay	5-40
Asphalt	4.5-6 (Zhao et al. 2018)
Flexible road base	8-12 (Zhao et al. 2018)
Gravel subgrade	8-15 (Zhao et al. 2018)
Iron	1.4-1.6 (Alsharahi et al. 2016)

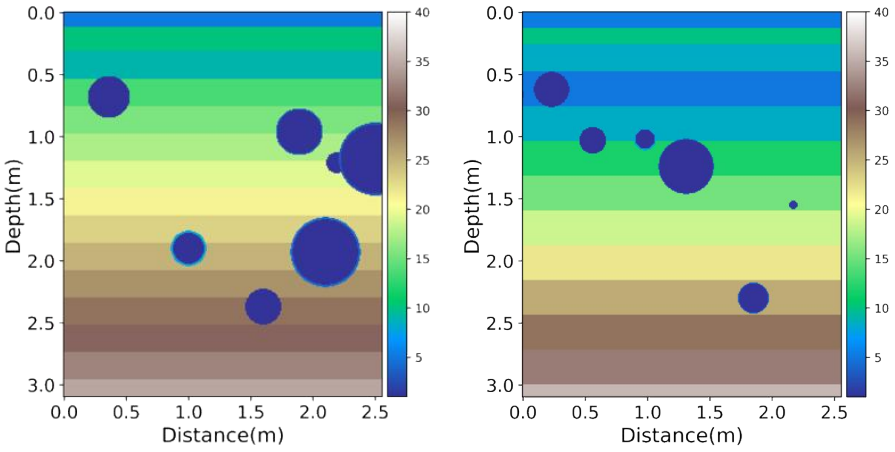

Figure 2: Examples of simulated permittivity map of subsurface with underground utilities. The color bar value and the different colors indicate the dielectric constant values.

Figure 2 presents two examples of simulated subsurface road layers with buried pipelines. Note that relative permittivity for the subgrade layer increases with increasing depth to account for density and water content variation.

The gprMax frequency used in this study is 350MHz, which is well accepted for GPR simulation. The 350 MHz antenna has a penetration depth of up to 10 meters. Therefore, the penetration depth of 350 MHz is suitable for subsurface mapping in the context of urban pavement. Each simulated permittivity map has 256 traces, and the total length is 2.56m. The depth of simulated models is set to 3.1m.

4.2 Data Preprocess

The simulated permittivity maps are in the spatial depth domain, which needs to be further converted into a time domain. Equation (1) gives the converting step, where t represents the two-way travel time in ns, d is depth in meters, ε stands for the dielectric constant, and C is the speed of light ($3 \times 10^8 m/s$).

$$t = \frac{2d}{c}\sqrt{\varepsilon} \tag{1}$$

The gprMax simulation spatial step is 1 cm, and the time window is 2.35865e-11s. The number of iterations is set as 3000, which is equivalent to a travel time of 70.76 ns. Time-zero correction is applied to eliminate the influence of the slight variations in the initiation time of the receiver and transmitter. The time-corrected radargram has an iteration of 2600 which is 61.32 ns. It is known that the amplitude of the transmitted signal diminishes as it gets deeper into the ground. This attenuation can make it difficult to recognize targets from GPR data, which could also affect the performance of network training. Therefore, an exponential gain was used to compensate for signal attenuation. Figure 3 shows two examples of the subsurface permittivity map and corresponding radargrams in the time-depth domain.

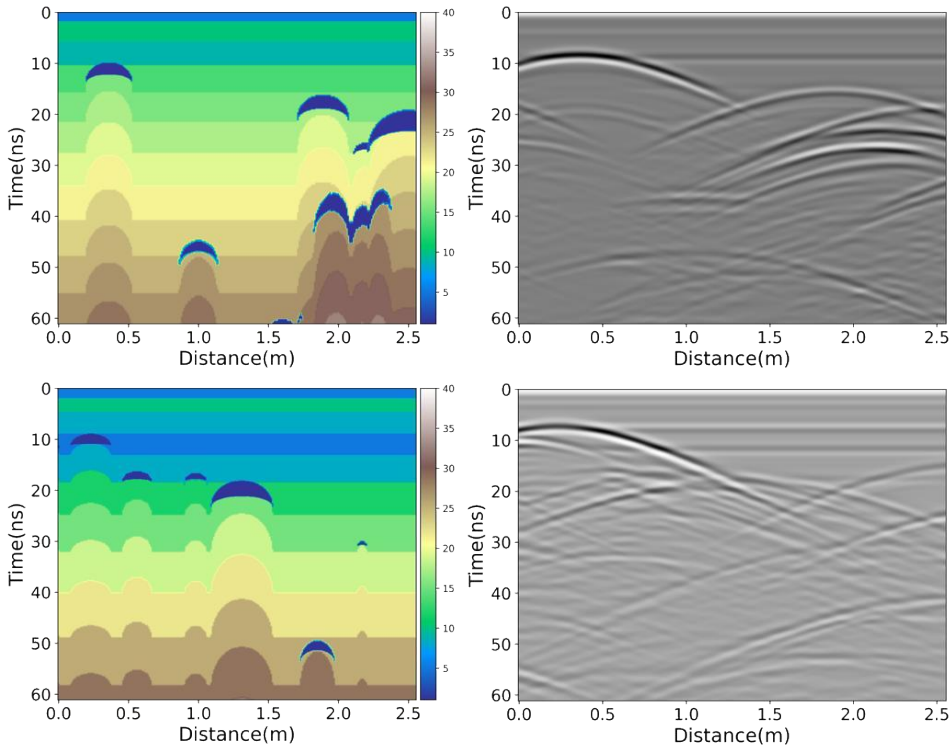

Figure 3: The down-sampled time-corrected radargram and permittivity map. The color bar value and the different colors indicate the dielectric constant values.

5 EXPERIMENT AND RESULTS

5.1 Implementation Details

The deep learning model was trained on a workstation with a 2.2 GHz Intel Xeon 10 Core CPU, 64 GB, and NVIDIA Quadro P5000 GPU using torch library on top of the PyTorch platform. The network was trained with an SGD optimizer (Bottou 2010) with a learning rate of 0.002. The learning rate decays with a factor of 0.5 using the ReduceLROnPlateau function in PyTorch with max mode and patience of 20. The batch size is set to 32. A total of 15,614 pairs of radargrams with ground-truth permittivity maps were generated to train the network. The dataset was randomly split into a training set (90%), and a validation set (10%).

5.2 Evaluation Metric

In this study, R^2, SSIM and MAE are used to evaluate the performance of the proposed deep learning inversion network. R^2 is used to measure the amount of variance in the predictions explained by the model, which is defined in Equation (2), where x_i represents the prediction value in the permittivity map, y_i represents the actual value in the original data, $\bar{y}$ represents the mean of all the actual values.

$$R^2 = \frac{SSR}{SST} = \frac{\sum(x_i - \bar{y})^2}{\sum(y_i - \bar{y})^2} \tag{2}$$

The image Structure Similarity (SSIM) calculates the structural similarities of different sliding windows in their corresponding positions between the original permittivity map and the predicted permittivity map. In Equation (3), x and y are the predicted map and original permittivity map, respectively (Yan et al. 2020).

$$SSIM(y, x|\omega) = \frac{(2\bar{\omega}_y\bar{\omega}_x + C_1)(2\sigma_{\omega_y\omega_x} + C_2)}{(\bar{\omega}_y^2 + \bar{\omega}_x^2 + C_1)(\sigma_{\omega_y}^2 + \sigma_{\omega_x}^2 + C_2)} \tag{3}$$

where C_1 and C_2 are two constants. ω_y is a sliding window in y, $\bar{\omega}_y$ represents the average of ω_y, $\sigma_{\omega_y}^2$ is the variance of ω_y and $\sigma_{\omega_y\omega_x}$ denotes the covariance of ω_y and ω_x. The variable ω_x, $\bar{\omega}_x$ and σ_{ω_x} have the same meaning in the x .

The Mean Absolute Error (MAE) denotes the average of all absolute errors which is calculated as Equation (4).

$$MAE = \frac{\sum_{i=1}^{n} abs(x_i - y_i)}{n} \tag{4}$$

5.3 Results

The following two figures show the training performance of the proposed network and the prediction results of the model. Figure 4 shows the variation of the three metrics R^2, SSIM, and MAE epochs during the training process. It is evident from the plot that the three metrics converge quickly and stably. As the epochs increase, the SSIM and R^2increase while the MAE decreases on both training and validation datasets. The best performance achieved on the validation dataset for R^2, SSIM and MAE are 0.96, 0.91, and 0.53, respectively, indicating the effectiveness of the proposed model.

Figure 5 presents two example inversion results. The predicted permittivity values in the prediction are in good agreement with the ground-truth permittivity map. The prediction permittivity map can be used to identify the subsurface structures, as well as recognize the location, size, and materials of buried utilities.

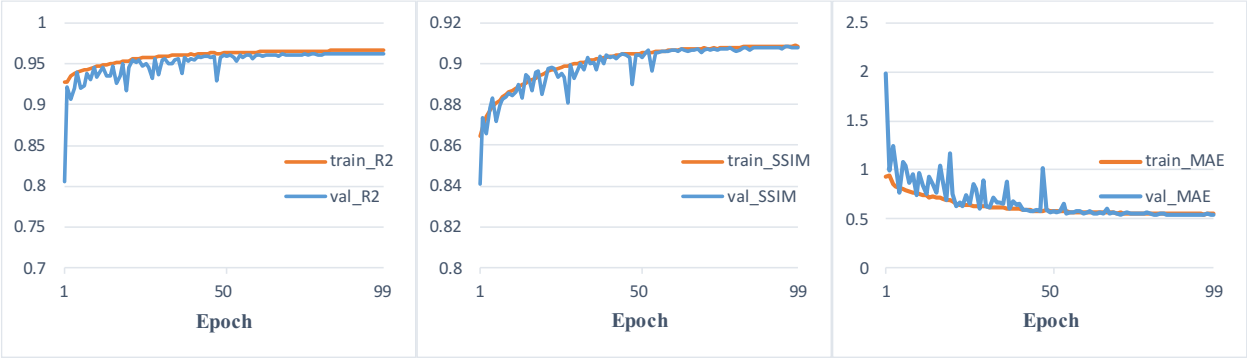

(a) (b) (c)

Figure 4: The R^2, SSIM, and MAE over epochs during training. (a) R^2; (b) SSIM; and (c) MAE

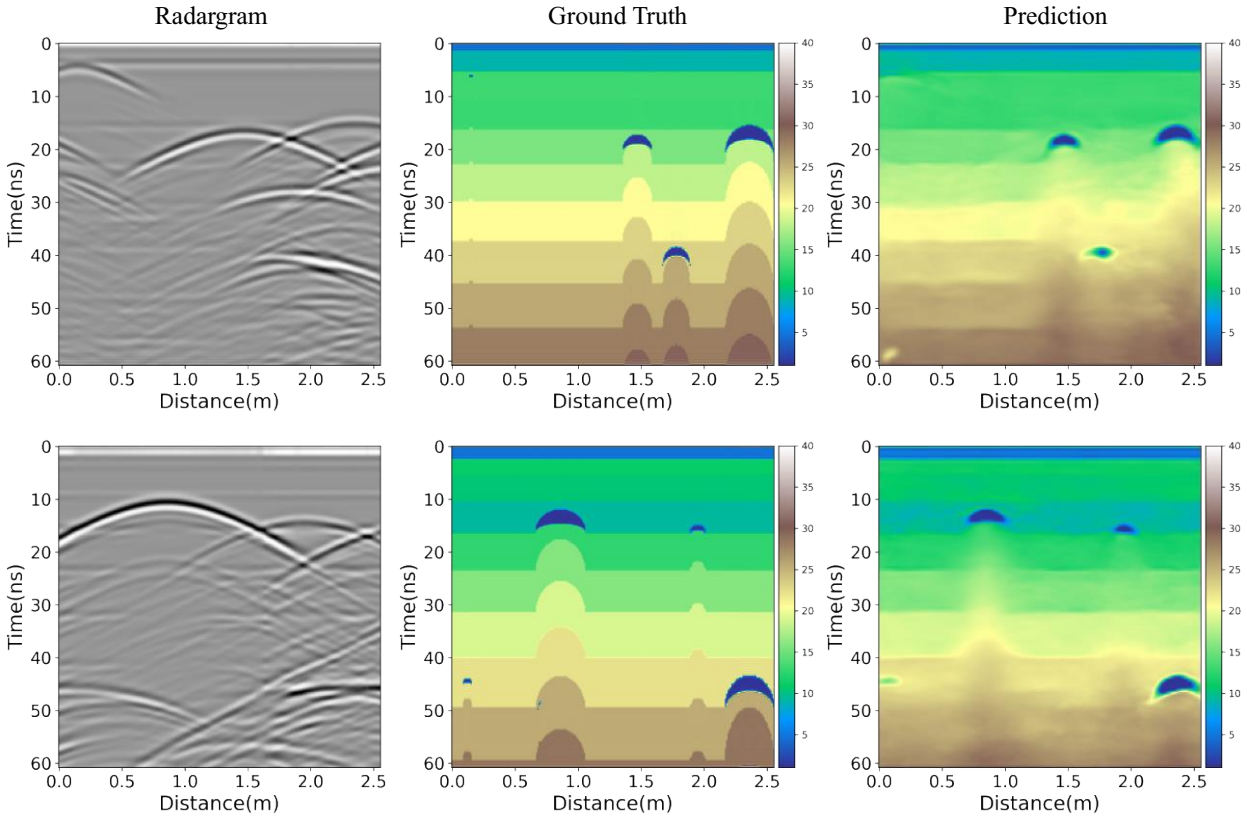

Figure 5: Example inversion results. The color bar value and the different colors indicate the dielectric constant values.

6 CONCLUSIONS AND FUTURE WORKS

Subsurface mapping has been an urging task for urban construction to decrease the excavation accident as well as build the foundation for a smart city. The overall goal of this research is to develop an algorithm for the detection and characterization of underground utilities from GPR scans. A novel encoder-decoder network was developed to directly reconstruct permittivity maps from GPR scans. To alleviate the issue of limited data, numerical simulation was adopted to generate synthetic GPR scans with corresponding

permittivity maps. The data preparation follows the regulation and standards to reflect realistic scenarios, facilitating the applicability of trained inversion networks in the real world. The developed method achieved an R^2 of 0.96, an SSIM of 0.91, and an MAE of 0.53 on the validation set of the synthetic dataset. The promising results highlight the potential of the proposed method in urban subsurface mapping.

The generalizability of these results is subject to certain limitations. First, this work only considered a relatively ideal subsurface environment without rocks and tree roots. In the future, more realistic data need to be generated for more robust performance in the real world. The realistic data can be generated by simulating the subsurface model with a realistic environment, such as adding stone and tree roots. Second, the inversion model was trained using the synthetic data only, compromising its performance in real-world applications. Augmenting synthetic GPR data with realistic signal characteristics is an interesting research direction to be explored. Third, while the proposed method achieves promising results in subsurface permittivity map reconstruction, the type of buried utilities is not analyzed in this work. In the future, it would be very useful to identify the type of underground utilities.

ACKNOWLEDGMENTS

This research was funded by the U.S. National Science Foundation (NSF) via Grant 1850008 and 2129003. The authors gratefully acknowledge NSF's support. Any opinions, findings, recommendations, and conclusions in this paper are those of the authors and do not necessarily reflect the views of NSF, The University of Tennessee, Knoxville, and The University of Texas at San Antonio.

REFERENCES

Ahmadi, R., and N. Fathianpour. 2017. "Estimating Geometrical Parameters of Cylindrical Targets Detected by Ground-Penetrating Radar Using Template Matching Algorithm". *Arabian Journal of Geosciences* 10(6):140.

Alsharahi, G., A. Driouach, and A. Faize. 2016. "Performance of GPR Influenced by Electrical Conductivity and Dielectric Constant". *Procedia Technology* 22:570–575.

American Society of Mechanical Engineers. 2016. "Pipeline Transportation Systems for Liquids and Slurries ASME Code for Pressure Piping". American Society of Mechanical Engineers.

Bottou, L. 2010. "Large-Scale Machine Learning with Stochastic Gradient Descent". In *Proceedings of COMPSTAT'2010*, edited by Y. Lechevallier and G. Saporta, 177-186. Heidelberg: Physica-Verlag HD.

Bruschini, C. 2000. "Metal Detectors in Civil Engineering and Humanitarian Demining: Overview and Tests of A Commercial Visualizing System". *INSIGHT-Non-Destructive Testing and Condition Monitoring* 42(2).

Chen, L.-C., Y. Zhu, G. Papandreou, F. Schroff, and H. Adam. 2018. "Encoder-Decoder with Atrous Separable Convolution for Semantic Image Segmentation". In *Proceedings of the European Conference on Computer Vision (ECCV)*, edited by V. Ferrari, M. Hebert, C. Sminchisescu, and Y. Weiss, 801-818. Cham, Switzerland: Springer Nature Switzerland AG.

Das, Y. 2006. "Effects of Soil Electromagnetic Properties on Metal Detectors". *IEEE Transactions on Geoscience and Remote Sensing* 44(6):1444–1453.

Feng, J., L. Yang, H. Wang, Y. Song, and J. Xiao. 2020. "GPR-based Subsurface Object Detection and Reconstruction Using Random Motion and DepthNet". In *2020 IEEE International Conference on Robotics and Automation (ICRA)*, edited by A. Howard, 7035-7041. Piscataway, New Jersey: Institute of Electrical and Electronics Engineers, Inc.

Folkman, S. 2014. "Validation of the Long Life of PVC Pipes". In *Proceedings of the 17th International Conference on Plastics Pipes*, September 22nd-24th, Chicago, USA.

He, K., X. Zhang, S. Ren, and J. Sun. 2016. "Deep Residual Learning for Image Recognition". In *Proceedings of the IEEE Conference on Computer Vision and Pattern Recognition*, edited by L. O'Conner, 770-778. Piscataway, New Jersey: Institute of Electrical and Electronics Engineers, Inc.

Hilario, M. S., B. W. Hoff, B. Jawdat, M. T. Lanagan, Z. W. Cohick, F. W. Dynys, J. A. Mackey, and J. M. Gaone. 2019. "W-Band Complex Permittivity Measurements at High Temperature Using Free-Space Methods". *IEEE Transactions on Components, Packaging and Manufacturing Technology* 9(6):1011–1019.

Hou, F., W. Lei, S. Li, and J. Xi. 2021. "Deep Learning-Based Subsurface Target Detection from GPR Scans". *IEEE Sensors Journal* 21(6):8161–8171.

Hu, D., J. Chen, and S. Li. 2022. "Reconstructing Unseen Spaces in Collapsed Structures for Search and Rescue via Deep Learning Based Radargram Inversion". *Automation in Construction* 140:104380.

Hu, D., L. Chen, J. Du, J. Cai, and S. Li. 2022. "Seeing through Disaster Rubble in 3D with Ground-Penetrating Radar and Interactive Augmented Reality for Urban Search and Rescue". *Journal of Computing in Civil Engineering* 36(5):04022021.

Hu, D., and S. Li. 2022. "Recognizing Object Surface Materials to Adapt Robotic Disinfection in Infrastructure Facilities". *Computer-Aided Civil and Infrastructure Engineering*.

Hu, D., S. Li, J. Chen, and V. R. Kamat. 2019. "Detecting, Locating, and Characterizing Voids in Disaster Rubble for Search and Rescue". *Advanced Engineering Informatics* 42:100974.

Hu, D., H. Zhong, S. Li, J. Tan, and Q. He. 2020. "Segmenting Areas of Potential Contamination for Adaptive Robotic Disinfection in Built Environments". *Building and Environment* 184:107226.

Ji, Y., F. Zhang, J. Wang, Z. Wang, P. Jiang, H. Liu, and Q. Sui. 2021. "Deep Neural Network-Based Permittivity Inversions for Ground Penetrating Radar Data". *IEEE Sensors Journal* 21(6):8172–8183.

Lester, J., and L. E. Bernold. 2007. "Innovative Process to Characterize Buried Utilities Using Ground Penetrating Radar". *Automation in Construction* 16(4):546–555.

Li, S., H. Cai, M. Abraham Dulcy, and P. Mao. 2016. "Estimating Features of Underground Utilities: Hybrid GPR/GPS Approach". *Journal of Computing in Civil Engineering* 30(1):04014108.

Li, S., H. Cai, and V. R. Kamat. 2015. "Uncertainty-Aware Geospatial System for Mapping and Visualizing Underground Utilities". *Automation in Construction* 53:105–119.

Liu, B., Y. Ren, H. Liu, H. Xu, Z. Wang, A. G. Cohn, and P. Jiang. 2021. "GPRInvNet: Deep Learning-Based Ground-Penetrating Radar Data Inversion for Tunnel Linings". *IEEE Transactions on Geoscience and Remote Sensing* 59(10):8305–8325.

Metje, N., B. Ahmad, and S. M. Crossland. 2015. "Causes, Impacts and Costs of Strikes on Buried Utility Assets". *Proceedings of the Institution of Civil Engineers-Municipal Engineer* 168(3):165-174.

National Academy of Engineering. 2019. Grand Challenges - 14 Grand Challenges for Engineering. http://www.engineeringchallenges.org/challenges.aspx, accessed 17th April.

Pasolli, E., F. Melgani, and M. Donelli. 2009. "Automatic Analysis of GPR Images: A Pattern-Recognition Approach". *IEEE Transactions on Geoscience and Remote Sensing* 47(7):2206–2217.

Pipeline and Hazardous Materials Safety Administration. 2021. Pipeline Incident 20 Year Trends. https://www.phmsa.dot.gov/data-and-statistics/pipeline/pipeline-incident-20-year-trends, accessed 17th April.

Qin, H., Y. Tang, Z. Wang, X. Xie, and D. Zhang. 2021. "Shield Tunnel Grouting Layer Estimation Using Sliding Window Probabilistic Inversion of GPR Data". *Tunnelling and Underground Space Technology* 112:103913.

Rajiv, K., G. R. Chandra, and B. B. Rao. 2017. "GPR Objects Hyperbola Region Feature Extraction". *Advances in Computational Sciences and Technology* 10(5):789–804.

Rohman, B. P. A., and M. Nishimoto. 2021. "Basic Shape Classification of Buried Object Using Pattern Matching in Ultrawideband Radar Image". In *2020 International Symposium on Antennas and Propagation (ISAP)*, January 25th-28th, Osaka, Japan, 739-740.

Sagnard, F., and J.-P. Tarel. 2016. "Template-Matching Based Detection of Hyperbolas in Ground-Penetrating Radargrams for Buried Utilities". *Journal of Geophysics and Engineering* 13(4):491–504.

Singh, N. P., and M. J. Nene. 2013. "Buried Object Detection and Analysis of GPR Images: Using Neural Network and Curve Fitting". In *2013 Annual International Conference on Emerging Research Areas and 2013 International Conference on Microelectronics, Communications and Renewable Energy*, June 4th-6th, Kanjirapally, India, 1-6.

Sterling, R. L., J. Anspach, E. Allouche, J. Simicevic, C. D. Rogers, K. E. Weston, and K. Hayes. 2009. "Encouraging Innovation in Locating and Characterizing Underground Utilities". Technical Report SHRP 2 Report S2-R01-RW, Transportation Research Board.

Su, X., S. Talmaki, H. Cai, and V. R. Kamat. 2013. "Uncertainty-Aware Visualization and Proximity Monitoring in Urban Excavation: A Geospatial Augmented Reality Approach". *Visualization in Engineering* 1(1):2.

Talmaki, S., and V. R. Kamat. 2014. "Real-Time Hybrid Virtuality for Prevention of Excavation Related Utility Strikes". *Journal of Computing in Civil Engineering* 28(3):04014001.

Tennessee Department of Transportation. 2021. "Tennessee Department of Transportation Standard Specification for Road and Bridge Construction". Tennessee Department of Transportation.

Thomas, A. M., C. D. F. Rogers, D. N. Chapman, N. Metje, and J. Castle. 2009. "Stakeholder Needs for Ground Penetrating Radar Utility Location". *Journal of Applied Geophysics* 67(4):345–351.

Warren, C., A. Giannopoulos, and I. Giannakis. 2016. "gprMax: Open Source Software to Simulate Electromagnetic Wave Propagation for Ground Penetrating Radar". *Computer Physics Communications* 209:163–170.

Westwańska, W., and J. Respondek. 2020. "Machine Learning in Object Recognition and Segmentation by Certain Class Neural Networks". In *2020 20th International Conference on Computational Science and Its Applications (ICCSA)*, July 1st-4th, Cagliari, Italy, 67-73.

Westwańska, W. W., and J. S. Respondek. 2019. "Counting Instances of Objects in Color Images Using U-Net Network on Example of Honey Bees". In *2019 Federated Conference on Computer Science and Information Systems (FedCSIS)*, September 1st-4th, Leipzig, Germany, 87-90.

Yamaguchi, T., T. Mizutani, and T. Nagayama. 2021. "Mapping Subsurface Utility Pipes by 3-D Convolutional Neural Network and Kirchhoff Migration Using GPR Images". *IEEE Transactions on Geoscience and Remote Sensing* 59(8):6525–6536.

Yan, X., S. Z. Gilani, H. Qin, and A. Mian. 2020. "Structural Similarity Loss for Learning to Fuse Multi-Focus Images". *Sensors* 20(22):6647.

Yang, F., X. Qiao, Y. Zhang, and X. Xu. 2014. "Prediction Method of Underground Pipeline Based on Hyperbolic Asymptote of GPR Image". In *Proceedings of the 15th International Conference on Ground Penetrating Radar*, June 30th-July 4th, Brussels, Belgium, 674-678.

Zhao, S., Y. Sun, Y. Zhou, and X. Han. 2018. "Experimental Study on Dielectric Properties of Pavement Structure Layer Based on Radar Image". *Chemical Engineering Transactions* 66:883-888.

AUTHOR BIOGRAPHIES

MENGJUN WANG is a Ph.D. student in the Department of Civil and Environmental Engineering at the University of Tennessee, Knoxville. She graduated from Changsha University of Science & Technology with a bachelor's degree in Traffic Engineering. Her research interests include automation in construction and construction informatics. Her e-mail address is mwang43@vols.utk.edu.

DA HU is a Ph.D. candidate in the Department of Civil and Environmental Engineering at the University of Tennessee, Knoxville. He holds a master's degree in Civil Engineering from Texas Tech University and a master's degree in Disaster Prevention and Reduction Engineering and Protective Engineering from the University of Chinese Academy of Sciences. His research interests include automation in construction, construction robotics, and disaster response. His e-mail address is dhu5@vols.utk.edu.

SHUAI LI is an assistant professor in the Department of Civil and Environmental Engineering at the University of Tennessee, Knoxville. He graduated from Purdue University with a Ph.D. degree in Civil Engineering, a master's degree in industrial engineering, and a master's degree in economics. He conducts fundamental research in sensing, automation, robotics, and visualization, and applies the techniques in numerous applications, including smart construction, disaster response, and manufacturing. His e-mail address is sli48@utk.edu.

JIANNAN CAI is an assistant professor in the School of Civil & Environmental Engineering, and Construction Management at the University of Texas at San Antonio. She holds a Ph.D. degree in Civil Engineering from Purdue University and an M.S. degree in Civil Engineering from Tongji University. Her research interests include data sensing and analysis, computer vision, deep learning, and robotics in construction, infrastructure, and building engineering and management. Her e-mail address is jiannan.cai@utsa.edu.